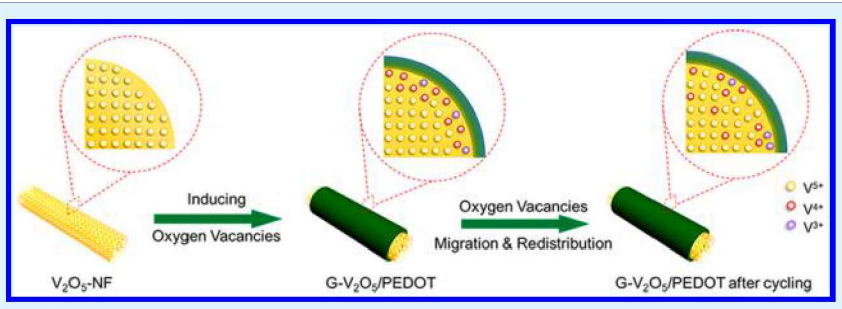
Gradient Oxygen Vacancies in V₂O₅/PEDOT Nanocables for High-Performance Supercapacitors

Wenchao Bi, †,‡ Yingjie Wu, $^{\$}$ Chaofeng Liu, ‡ Jichao Wang, † Yuchuan Du, $^{\parallel}$ Guohua Gao, *,† Guangming Wu, *,† and Guozhong Cao $^{*,\ddagger_{0}}$

Supporting Information



ABSTRACT: $V_2O_5/\text{poly}(3,4\text{-ethylenedioxythiophene})$ nanocables with oxygen vacancies gradually decreasing from the surface to the core (G- V_2O_5/PEDOT nanocables) were prepared as electrodes for supercapacitors. Gradient oxygen vacancies formed when 3,4-ethylenedioxythiophene monomers polymerized conformally on the surface of V_2O_5 nanofibers, providing G- V_2O_5/PEDOT nanocables with much improved charge storage kinetics and structural durability. The role of gradient oxygen vacancies in enhancing charge transfer/transport was also evidenced by means of density functional theory calculations. G- V_2O_5/PEDOT nanocable-based supercapacitors showed excellent electrochemical performance with a high specific capacitance of 614 F g⁻¹ and energy density of 85 W h kg⁻¹ in neutral aqueous electrolyte. The synergistic combination of gradient oxygen vacancies and polymer shell provided the G- V_2O_5/PEDOT nanocable-based supercapacitors with an excellent long cycling life with 122% capacitance retention after 50 000 cycles. Without any additional oxidizing agent, this simple synthesis method is cost competitive and ready for scale up manufacturing for such energy storage electrode materials.

KEYWORDS: gradient oxygen vacancies, vanadium pentoxide, PEDOT, nanocables, supercapacitors

1. INTRODUCTION

Renewable and sustainable energy has attracted much research and commercialization interest due to increasing environmental concerns, and energy storage technologies capable of high energy and high power densities are imperatively needed to meet the rapid increasing energy demands. 1-4 Supercapacitors are attractive as electrochemical energy storage devices in applications such as electric cars, due to their high power density, good charge/discharge rates, and long cycling life.5,6 However, a higher energy density is required for supercapacitors to achieve wider applications. To date, significant attention has been paid to explore and develop electrode materials for high-performance supercapacitors.^{7–9} Among these supercapacitor electrode materials, pseudocapacitive transition-metal oxides and conducting polymers have been extensively studied, and fast faradaic reactions render much higher specific capacitance and energy density than those

purely based on electric double-layer capacitive (EDLC) carbon-based materials. ^{10–13}

Vanadium pentoxide (V_2O_5), a transition-metal oxide, is promising for its low cost, material abundance, multiple oxidation states (V–II) that create a wide potential window, and high theoretical capacitance. However, V_2O_5 as a supercapacitor electrode material suffers from its intrinsically low electrical conductivity ($4 \times 10^{-4} \ {\rm S \ cm^{-1}}$) and electrochemical instability caused by chemical dissolution or structural pulverization during fast charge/discharge cycling. The poor electrical conductivity can greatly retard the practical capacitive performance of V_2O_5 with poor charge transfer/transport, and soluble species (e.g., $H_2VO_4^-$, $HV_2O_5^-$, VO^{2+}) which form in aqueous electrolyte during cycling

Received: October 4, 2018 Accepted: December 3, 2018 Published: December 3, 2018



[†]Shanghai Key Laboratory of Special Artificial Microstructure Materials and Technology, School of Physics Science and Engineering, Tongji University, Shanghai 200092, China

[‡]Department of Materials Science and Engineering, University of Washington, Seattle, Washington 98195-2120, United States §Department of Materials Science and Engineering, Monash University, Clayton, Victoria 3800, Australia

Key Laboratory of Road and Traffic Engineering of the Ministry of Education, Tongji University, Shanghai 201804, China

processes will affect the morphology and crystal structure of vanadium oxides and lead to a serious capacity degradation. 22,23 Various strategies have been studied to improve the electrochemical properties and device performance. For example, nanostructured V2O5 with much increased specific surface area or surface to volume ratio and much reduced dimension for short transport distance has been demonstrated to be effective in improving both the electrochemical properties and the device performance.²⁴ Engineering the surface chemistry has been another active research direction, such as through the introduction of a surface carbonaceous coating or surface defects. Introducing oxygen vacancies into transition-metal oxides, such as MoO₃ and MnO₂, ^{25,26} has been reported as an effective strategy to retain the structures, improve the intrinsic conductivity, and promote pseudocapacitive charge storage kinetics of redox-active materials, because oxygen vacancies can change the structural and charge storage properties of electrode materials. Research studies on V₂O₅ lithium-ion batteries also show that oxygen vacancies on the V₂O₅ surface could improve the intrinsic conductivity and the cycling stability of 1V_2O_5 during repeated lithium-ion intercalation/deintercalation processes. A proper ratio of low vanadium valence states (like V4+) in vanadium oxide supercapacitor electrode materials also can restrain instability so that there is better pseudocapacitive performance.² Therefore, creating oxygen vacancies in V₂O₅ and the corresponding reduced vanadium ions should be feasible for enhancing the electrochemical performance of supercapacitors.

Despite a long study of oxygen vacancies in V₂O₅ for batteries, most oxygen vacancies were created by heating V₂O₅ under vacuum, inert, or reducing conditions (e.g., N_2 or H_2); electrochemical reduction and self-dropping,³⁰ and the effects of oxygen vacancies caused by chemical reduction, especially by the oxidative polymerization of conducting polymers, on supercapacitor electrode materials need to be further explored. Moreover, the distribution of oxygen vacancies is difficult to control directly. When the polymerization of conducting polymers starts from the surface of V2O5, like upon building a core-shell structure, the chemical reduction caused oxygen vacancies in V₂O₅ that might possess an ordered distribution. At the same time, core—shell V_2O_5 /polypyrrole nanoribbons³¹ confirm that the polypyrrole coating can extrinsically improve electrical conductivity and prevent V2O5 from pulverizing. However, their electrochemical performance (308 F g⁻¹ at 100 $mA g^{-1}$, 42 W h kg^{-1}) still cannot meet daily requirements, and the synthesis is complicated because the polymerization of conductive polymer requires additional surfactant and/or oxidants (such as anionic dodecylbenzenesulfonate, FeCl₃). Since multifunctional properties of materials can significantly enhance the electrochemical performance via the synergistic influences between intrinsic and extrinsic improvements, it is of great significance to identify the contribution of polymerization-induced oxygen vacancies to the surface morphology and electrochemical performance of vanadium-based electrode materials for better energy storage devices.

In this work, a gradient distribution of oxygen vacancies is induced in V₂O₅ nanofibers (V₂O₅-NF) via the *in situ* polymerization of poly(3,4-ethylenedioxythiophene) (PEDOT) at the surface of V₂O₅-NF to significantly boost the charge transfer and stability of V₂O₅-NF. PEDOT is used because its doped state possesses remarkable conductivity (300–500 S cm⁻¹) and stability over other doped conducting polymer families, such as polypyrrole (PPy, 10–50 S cm⁻¹)

and polyaniline (PANI, 0.1-5 S cm⁻¹). Gradient oxygenvacant V₂O₅/poly(3,4-ethylenedioxythiophene) (denoted as G-V₂O₅/PEDOT) nanocables are synthesized by a vaporphase polymerization method, which ensures a homogeneous PEDOT layer and renders V₂O₅-NF a gradually reduced concentration of oxygen vacancies from the surface to the inner volume. The vacuum system allows the preparation of G-V₂O₅/PEDOT under mild conditions (80 °C). The synthesis process becomes simple without involving additional oxidizing agents. Gradient oxygen vacancies and PEDOT shells of G-V₂O₅/PEDOT nanocables cause changes not only in their surface morphology, but also in their electrochemical performance. Applied in supercapacitors, G-V₂O₅/PEDOT nanocables exhibited superior specific capacitance and excellent cycling stability without capacitance decay after 50 000 cycles. Density functional theory calculations were performed and showed the role of oxygen vacancies in enhancing the charge transfer of V₂O₅. The morphology and oxygen vacancies of G-V₂O₅/ PEDOT nanocables after cycling were further investigated for the excellent cycling performance.

2. EXPERIMENTAL SECTION

2.1. Synthesis of G-V₂O₅/PEDOT Nanocables. G-V₂O₅/ PEDOT nanocables with a gradient distribution of oxygen vacancies were prepared by a vapor-phase polymerization method. First, a glass reactor containing V2O5-NF prepared according to a reported method³² was evacuated by a pump at room temperature (25 °C). Then, 0.5 mL of a hydrochloric acid (HCl, 36 wt %) solution was injected into the sealed container after the system reached vacuum conditions. Vapor-phase HCl filled the container and diffused into the V₂O₅-NF skeleton to sufficiently acidify the V₂O₅-NF. About 1 h later, the acidified V₂O₅-NF was transferred to another container and evacuated again, and then 0.5 mL of poly(3,4-ethylenedioxythiophene) monomers was added into this reactor at 80 °C. Vaporized monomers diffused into the inner regions of the V2O5-NF and polymerized as it deposited on the V₂O₅-NF surface. The color of the sample changed from yellow to dark green after 6 h, suggesting the successful formation of G-V₂O₅/PEDOT nanocables. The G-V₂O₅/ PEDOT nanocables were cooled in air for a few hours and then heated in a vacuum oven at 80 °C for 12 h.

2.2. Chemical and Structural Characterizations. The morphologies and structures of the samples were systematically investigated by field emission scanning electron microscopy (FESEM, S-4800), high-resolution transmission electron microscopy (HRTEM, field emission JEOL-2100), and transmission electron microscopy (TEM, JEOL-2100). Fourier transform infrared spectroscopy (FTIR) was measured by a Bruker-TENSOR27 FTIR spectrometer in the range 400-4000 cm⁻¹. X-ray powder diffraction (XRD) patterns were obtained by using a Rigaku D/max-C diffractometer with a Cu Kα radiation source ($\lambda = 1.5406$ Å). X-ray photoelectron spectroscopy (XPS) experiments were carried out on RBD upgraded PHI-5000C ESCA system (PerkinElmer) with Mg K α radiation ($h\nu$ = 1,253.6 eV). Thermogravimetric and differential scanning calorimetry (TG-DSC) analyses were carried out on SDT Q600 over the temperature range from 25 to 800 °C at a heating rate of 10 °C min⁻¹ in flowing air. The X-ray absorption near edge structure (XANES) measurements of the vanadium K-edge were performed at the University of Washington using laboratory-based instrumentation (see Supporting Information).

2.3. Electrochemical Property and Performance Measurements. A symmetrical two-electrode configuration was used to measure the performance of an electrode material's electrochemical performance with 1 M Na₂SO₄ aqueous solution as the electrolyte. ^{33,34} The electrodes were prepared with active materials, acetylene black and poly(vinylidene fluoride) (PVDF) in *N*-methylpyrrolidone (NMP) mixed at a mass ratio of 8:1:1. The obtained mixed slurry was used to coat 1 cm² of a 1 cm × 3 cm strip of graphite paper. These electrodes were dried at 120 °C for 12 h under vacuum. The loading

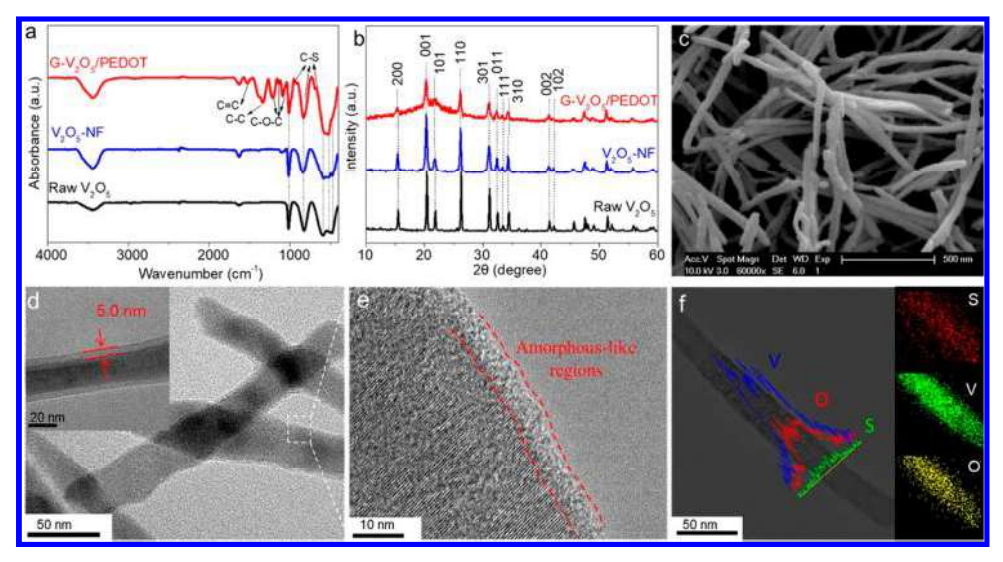


Figure 1. (a) FTIR spectra; (b) XRD patterns of as-prepared $G-V_2O_5/PEDOT$ nanocables, V_2O_5 powder, and V_2O_5-NF ; (c) SEM image; (d) TEM image; (e) HR-TEM images; and (f) SEDS line scanning profile and corresponding element mapping profiles of $G-V_2O_5/PEDOT$ nanocables with a uniform PEDOT coating.

of mixed materials is about 1 mg. The potential of the samples as electrode materials applied to symmetrical two-electrode supercapacitors was evaluated by cyclic voltammetry (CV), galvanostatic charge/discharge, and electrochemical impedance spectroscopy (EIS). CV and galvanostatic charge/discharge measurements were carried out with a CHI 660C electrochemical workstation, with a potential range of -1 to 1 V.35 The specific capacitance of a single electrode (C, F g⁻¹) was calculated from the galvanostatic discharge curves by the formula $C = 2I\Delta t/\Delta V$, where I was the constant discharging current density based on the total mass of a single electrode, Δt was the discharging time, and ΔV was the potential window. The energy density (E, W h kg⁻¹) and average power density (P, W kg⁻¹) of the device in Ragone plots were calculated with the formula E = (1/8) $C(\Delta V)^2/3600$ and $P = E/\Delta t$, respectively. EIS measurements were performed in a CHI 660C electrochemical workstation in the frequency range 0.01 Hz to 100 kHz with a ac amplitude of 5 mV.34 To investigate the improvement in the electrochemical performance, raw V₂O₅ powder and V₂O₅-NF were also tested under the same condition for supercapacitors.

3. RESULTS AND DISCUSSION

Fourier transform infrared spectroscopy (FTIR) results of G-V₂O₅/PEDOT nanocables, V₂O₅-NF, and raw V₂O₅ are shown in Figure 1a. For all the samples, the peaks at 1628 and 3440 cm⁻¹ are caused by the stretching and bending vibration modes of H-O and H-O-H bonds in absorbed or bound water molecules. The feature peaks of G-V₂O₅/PEDOT nanocables at 1016, 833, 613, 528, and 416 cm⁻¹ correspond to the vibration modes of terminal oxygen bonds, doubly coordinated oxygen (bridge oxygen) bonds, and triply coordinated oxygen (chain oxygen) bonds in raw V₂O₅ and V₂O₅-NF, respectively, showing the existence of V₂O₅ in the composite.³⁶ The presence of PEDOT is confirmed by peaks at 1522 and 1397 cm⁻¹ caused by aromatic C=C and C—C stretching in the thiophene rings; peaks at 1207, 1143, and 1090 cm⁻¹ assigned to C—O—C bond stretching; and peaks at 934, 833, and 692 cm⁻¹ which are related to C-S bond stretching vibrations in the thiophene rings.³⁷ All peaks in the G-V₂O₅/PEDOT structures display the successful compositing of V₂O₅ and PEDOT. The X-ray diffraction (XRD) profile in Figure 1b shows the crystallographic information on G-V₂O₅/ PEDOT composites. Compared to the raw V₂O₅ powder and

V₂O₅-NF, no obvious change in the position of diffraction peaks suggests that G-V₂O₅/PEDOT nanocables retain the main crystalline phase of V₂O₅-NF. Relatively broader peaks in G-V₂O₅/PEDOT nanocables indicate an amorphous phase existing in G-V₂O₅/PEDOT nanocables, which can be attributed to oxygen vacancies and PEDOT.³⁶ Similar to the scanning electron microscopy (SEM) image of V₂O₅-NF (Figure S1a), the SEM image in Figure 1c exhibits a smooth surface of G-V₂O₅/PEDOT nanocables without agglomeration. Transmission electron microscopy (TEM) images of G-V₂O₅/ PEDOT in Figure 1d directly deliver a nanocable structure with a dark core and a pale coating layer at a uniform thickness of 5.0 nm. The HRTEM image (Figure 1e) reveals that the core is a crystalline phase with lattice fringes corroborating with the XRD result. The interface between the core and the shell appears disordered without an obvious boundary, probably attributable to the large quantity of oxygen vacancies. The TEM-EDS (energy-dispersive X-ray spectrometry) line scan profile of G-V₂O₅/PEDOT for sulfur (S), oxygen (O), and vanadium (V) and its corresponding element mapping profiles were presented in Figure 1f. In the EDS line scanning profile crossing the nanocable, the signals for O and V from V_2O_5 -NF are intense at the core region and relatively reduced at the edge region, and a broader peak for S in PEDOT remains at the same intensity across the diameter, signifying a uniform PEDOT coating for V₂O₅-NF. Consistent with the radial line scan profile, the corresponding element mapping profiles also present uniform element distributions of S, O, and V in G-V₂O₅/PEDOT nanocables. The distribution of S from PEDOT is wider than that of O and V from V₂O₅-NF. This uniformity arises from the deep penetration, deposition, and polymerization of vapor-phase monomers in the V2O5-NF internal skeleton. Thermogravimetry and differential scanning calorimetry (TG-DSC) results shown in Figure S2 indicate that the content of PEDOT in G-V₂O₅/PEDOT is approximately 25%.

As to the gradient distribution of oxygen vacancies in $GV_2O_5/PEDOT$ nanocables, detailed understanding and research were conducted. It is known that oxygen vacancies can be created by heating nanostructured oxides in an oxygen-deficient environment. In the present study, gradient oxygen

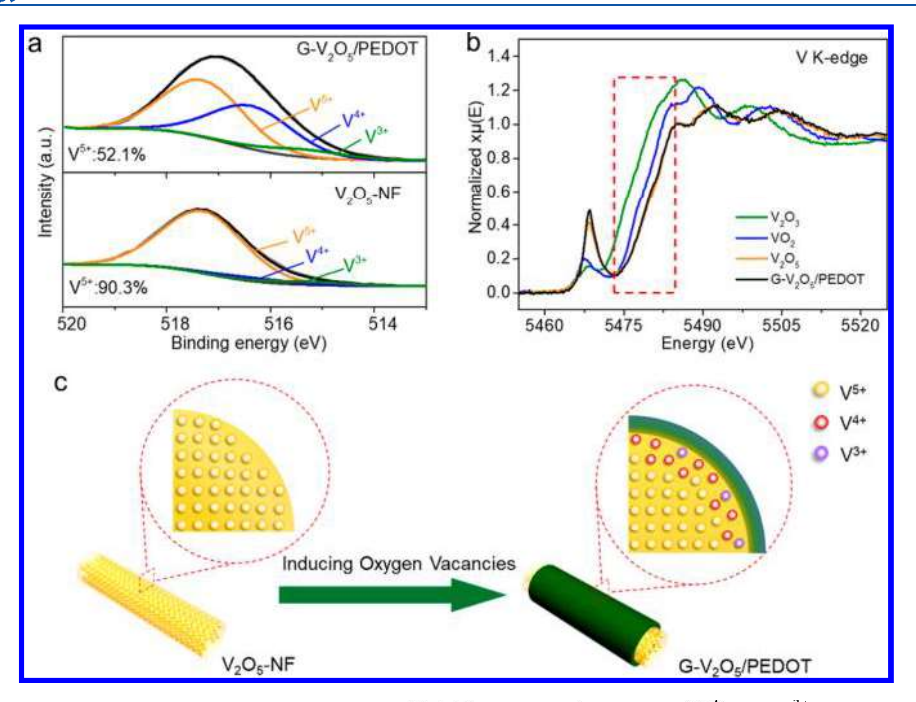


Figure 2. (a) XPS V $2p_{2/3}$ spectra of $G-V_2O_5/PEDOT$ and V_2O_5-NF . The increased content of V^{4+} and V^{3+} suggests the existence of gradient oxygen vacancies. (b) Normalized vanadium K-edge XANES spectrum of $G-V_2O_5/PEDOT$ as compared to several oxides. (c) Schematic illustrating the synthesis process of gradient oxygen vacancies in $G-V_2O_5/PEDOT$ nanocables.

vacancies are presumably obtained when 3,4-ethylenedioxythiophene monomers polymerize on the surface of V₂O₅-NF in vacuum. A stepwise reaction mechanism is widely accepted for the oxidative polymerization process of PEDOT where oxidants are usually involved.³⁹ Since no extra oxidizing agent was added in this experiment, it is reasonable to suppose that V_2O_5 -NF act as an oxidant to oxidize monomers to polymerize, leading to the formation of oxygen vacancies. It has been reported that V₂O₅ is one of the most easily reduced transitionmetal oxides, because it can easily lose a double-bonded oxygen atom leaving a terminal vanadium atom. 40 This terminal vanadium oxygen vacancy readily accepts and donates oxygen, making V₂O₅ a strong candidate for the oxidization of organic molecules. Thus, it is supposed that terminal vanadium oxygen vacancies form during a series of oxidizing. The synthesis process and structure are illustrated schematically in Figure 2c. As more monomer vapors deposit and undergo in situ oxidative polymerization along the backbone of V₂O₅-NF₁ more oxygen vacancies are created and G-V₂O₅/PEDOT nanocables are obtained. X-ray photoelectron spectroscopy (XPS) was used for hypothesis testing by analyzing the vanadium valence states associated with oxygen vacancies in G- $V_2O_5/PEDOT$ nanocables. The peak of V $2p_{3/2}$ is deconvoluted into three synthetic peaks of V^{5+} , V^{4+} , and V3+.29,32 The amount of vanadium of each valence state is calculated by comparing its corresponding peak area to the total vanadium peak areas (V $^{5+}$, V $^{4+}$, and V $^{3+}$) in XPS spectra (Figure 2a). As shown in Table 1, the content of V^{5+} reduces

Table 1. Changes in the Content of Vanadium Valence States from Gradient Oxygen Vacancies in $\text{G-V}_2\text{O}_5/\text{PEDOT}$ from XPS

sample	V^{5+}	V^{4+}	V^{3+}
V_2O_5 -NF	90.3%	5.0%	4.7%
G-V ₂ O ₅ /PEDOT	52.1%	40.6%	7.3%

from the original 90.3% in V₂O₅-NF to 52.1% in G-V₂O₅/ PEDOT, and the total valence decreases from 4.9 to 4.4 on the surface layer based on XPS analyses. It should be noted that although a large fraction of low-valence vanadium cations is measured in G-V₂O₅/PEDOT, the crystalline phase of V₂O₅ is retained as clearly indicated by the XRD patterns. These seemingly contradictory results are reasonable considering the fact that XPS measurements investigate the shallow surface. particularly considering the fact that there is a PEDOT shell of 5.0 nm. The surface layer might consist of a large fraction of oxygen vacancies since the polymerization occurs on the surface of V₂O₅-NF. However, with a low processing temperature, the diffusion of oxygen vacancies would be limited. The inner core of the V₂O₅-NF retains its original valence states and crystal structure, as shown in Figures 1e and 2c. Therefore, it is more likely that G-V₂O₅/PEDOT nanocables possess a concentration of oxygen vacancies gradually decreasing from the highest concentration at the surface, i.e., the interface between V₂O₅ and PEDOT, to nearly zero inside. This would also explain the fact that V⁵⁺, V⁴⁺, and V^{3+} coexist in the same sample, as it is likely the excessive oxidation at the surface that creates V4+ and V3+ at the subsurface, and V⁵⁺ inside the V₂O₅-NF. Since the XPS measurements characterized the shallow surface of G-V₂O₅/ PEDOT, X-ray absorption near edge structure (XANES) characterization was used to further investigate the vanadium oxidation states in the bulk, and the results are presented in Figure 2b. The energy position of the edge (highlighted with red), a known indicator of the oxidation state of a material, 41 is consistent between the G-V₂O₅/PEDOT and the V₂O₅ reference compound, confirming that the bulk of the sample is mainly composed of V₂O₅, which corroborates the HR-TEM and XRD analysis. Together with XPS analysis, the result further supports the gradient distribution of oxygen vacancies with V⁴⁺ and V³⁺ at the subsurface, and V⁵⁺ inside in G-V₂O₅/ PEDOT.

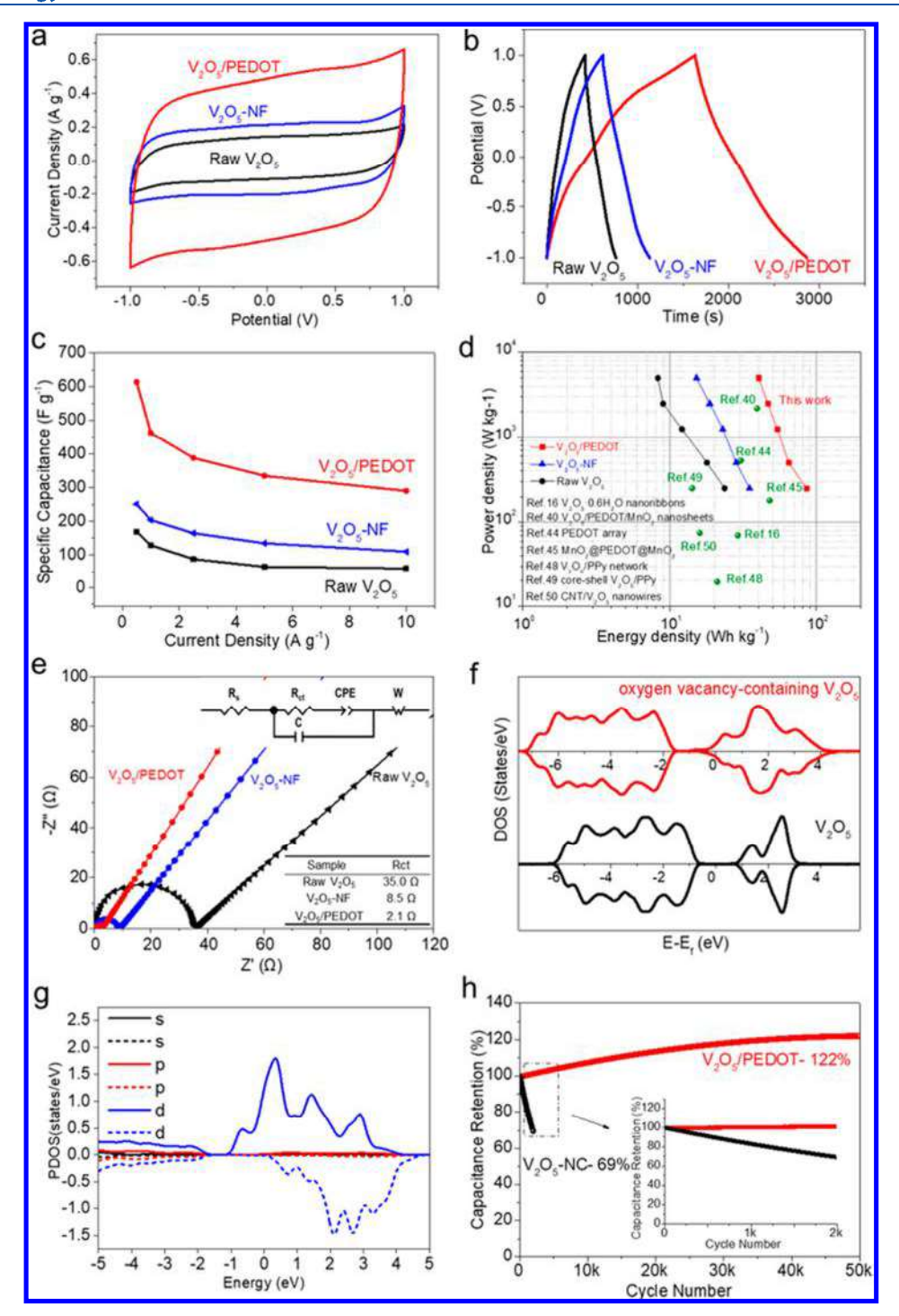


Figure 3. (a) CV curves of G-V₂O₅/PEDOT, V₂O₅-NF, and raw V₂O₅ at 5 mV s⁻¹. (b) Galvanostatic charge/discharge curves of G-V₂O₅/PEDOT, V₂O₅-NF, and raw V₂O₅ at 0.5 A g⁻¹. (c) Specific capacitances of G-V₂O₅/PEDOT, V₂O₅-NF, and raw V₂O₅ at different current densities. (d) Ragone plots of supercapacitors based on G-V₂O₅/PEDOT, V₂O₅-NF, and raw V₂O₅. Data of recently reported electrode materials are also illustrated for comparison, such as V₂O₅·0.6H₂O nanoribbons (29 W h kg⁻¹ at the power density of 70 W kg⁻¹), ¹⁶ V₂O₅/PEDOT/MnO₂ nanosheets (39 W h kg⁻¹ at the power density of 2200 W kg⁻¹), ⁴⁵ PEDOT array (30 W h kg⁻¹ at the power density of 529 W kg⁻¹), ⁴⁷ MnO₂@ PEDOT@MnO₂ (48 W h kg⁻¹ at the power density of 180 W kg⁻¹), ⁴⁸ V₂O₅/PPy network (21 W h kg⁻¹ at the power density of 19 kW kg⁻¹), ⁵¹ core/shell V₂O₅/PPy (14 W h kg⁻¹ at the power density of 250 W kg⁻¹), ⁵² and CNT/V₂O₅ nanowires (16 W h kg⁻¹ at the power density of 75 W kg⁻¹). ⁵³ (e) EIS spectra of G-V₂O₅/PEDOT, V₂O₅-NF, and raw V₂O₅ (the equivalent circuit model is inserted). (f) Calculated electronic DOS of stoichiometric V₂O₅ with terminal vanadium oxygen vacancies. (g) A PDOS calculation for the surface vanadium in vanadyl. (h) The cycling performance of G-V₂O₅/PEDOT and V₂O₅-NF. G-V₂O₅/PEDOT nanocables show a stable increase in capacitance retention over 50 000 charge/discharge processes.

 $G-V_2O_5/PEDOT$ nanocables were tested as supercapacitor electrodes in a symmetric two-electrode system with a 1 M Na_2SO_4 aqueous electrolyte. Raw V_2O_5 powder and V_2O_5-NF

were tested under the same conditions for comparison. The cyclic voltammetry (CV) curves of samples obtained at 5 mV s $^{-1}$ (Figure 3a) exhibit extremely symmetrical and nearly

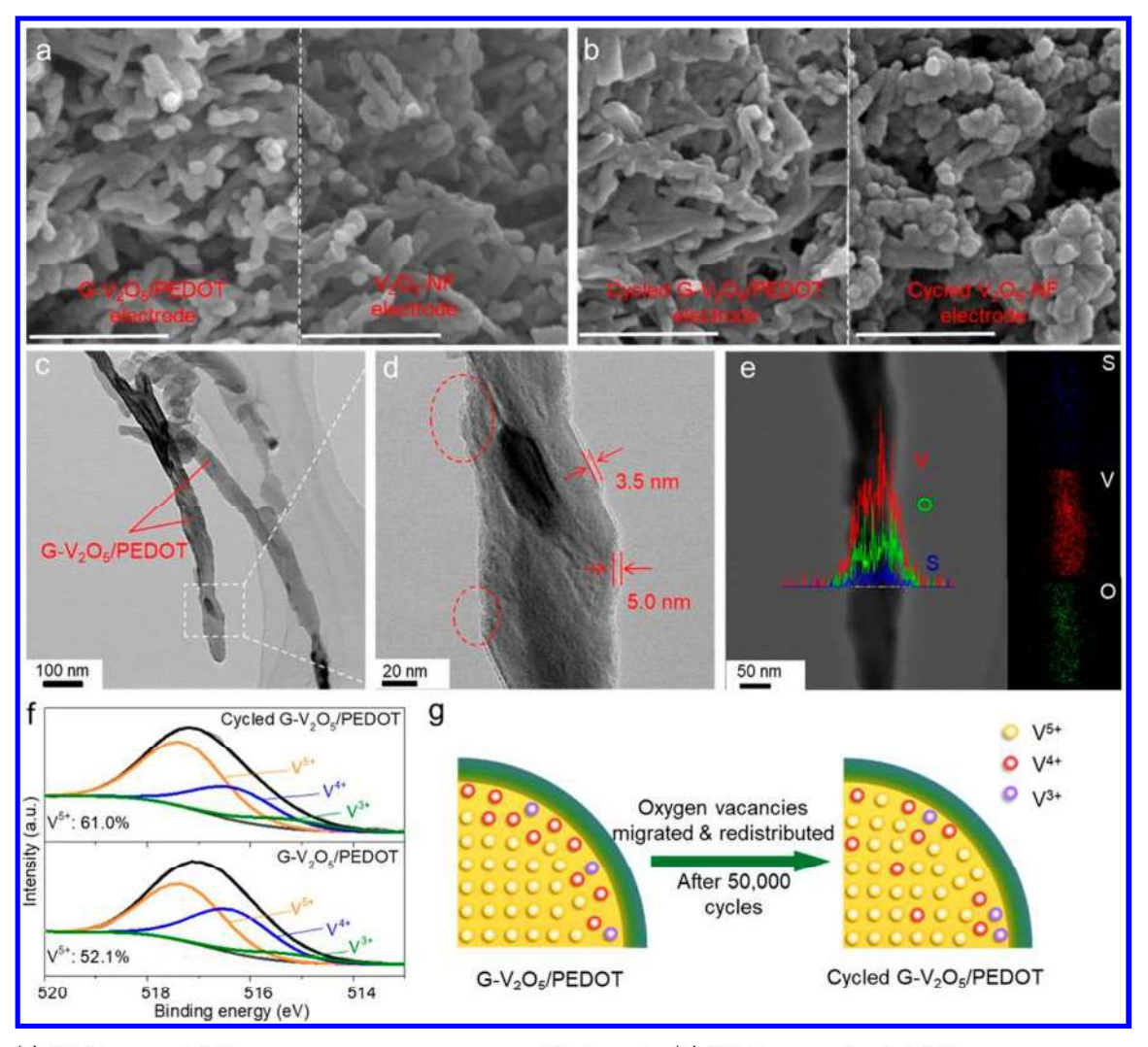


Figure 4. (a) SEM images of $G-V_2O_5$ /PEDOT electrode and V_2O_5 -NF electrode. (b) SEM images of cycled $G-V_2O_5$ -NF electrode after 50 000 cycles and cycled V_2O_5 -NF electrode after 2000 cycles. The scale bar is 500 nm. (c, d) TEM images and (e) EDS line scan and corresponding element mapping profiles of cycled $G-V_2O_5$ /PEDOT electrode. (f) XPS V $2p_{2/3}$ spectra of cycled $G-V_2O_5$ /PEDOT electrode with $G-V_2O_5$ /PEDOT as comparison. (g) Schematic illustrating the migration and redistribution of oxygen vacancies in cycled $G-V_2O_5$ /PEDOT electrode.

rectangular shapes, demonstrating the ideal capacitive performance. No obvious redox peaks are shown due to oxygen vacancies (low valence vanadium cations) at the surface of the G-V₂O₅/PEDOT nanocables.^{32,34} With an increased scan rate from 5 to 100 mV s⁻¹ the lack of significant distortion in the CV loops (Figure S3) indicates excellent kinetic reversibility and a high rate of the pseudocapacitive reactions. In agreement with CV curves, the galvanostatic charge/discharge curves of G-V₂O₅/PEDOT with nearly isosceles triangle shapes (Figure S4) further reveal high Coulombic efficiency, superior reversibility, and good charge propagation. The specific capacitance of G-V₂O₅/PEDOT nanocables is 614 F g⁻¹ at 0.5 A g⁻¹ calculated from galvanostatic charge/discharge curves (Figure 3b), while the value of raw V₂O₅ powder is only 170 F g⁻¹ and that for V₂O₅-NF is 251 F g⁻¹. This improved capacitive capability can be ascribed to the gradient oxygen vacancies and PEDOT shells, which will be discussed in the following paragraph. The specific capacitance of G-V₂O₅/PEDOT at various current densities and the Ragone plot are presented in Figure 3c,d, respectively. G-V₂O₅/PEDOT nanocables exhibit excellent electrochemical performance with an energy density of 85 W h kg⁻¹ when the power density is

250 W kg $^{-1}$, higher than that of raw V_2O_5 powder (24 W h kg $^{-1}$), V_2O_5 -NF (44 W h kg $^{-1}$), other vanadium-based materials, and PEDOT-based materials illustrated in the Ragone plot in Figure 3d. G- V_2O_5 /PEDOT nanocables hold great promise toward practical application in supercapacitors.

Electrochemical impedance spectroscopy (EIS) was employed to investigate the kinetic factors behind the significant increase in the electrochemical performance of G-V₂O₅/ PEDOT nanocables. In the Nyquist plots (Figure 3e), the G-V₂O₅/PEDOT curve possesses a steeper straight line in the low-frequency region, and a reduced charge transfer resistance (R_{ct}) value (2.1 Ω) compared to those of V_2O_5 -NF (8.5 Ω) and raw V_2O_5 (35.0 Ω) in the high-frequency region. The charge transfer kinetics at the G-V₂O₅/PEDOT electrodeelectrolyte interface is improved after the oxygen vacancies are created. 27,42 In this work, it is difficult to experimentally isolate the effects of the PEDOT coating, oxygen vacancies, and associated low-valence vanadium cations, because the gradient oxygen vacancies and reduced vanadium are created by the polymerization of PEDOT. On the basis of the previous research studies, all can improve the charge transfer kinetics of V₂O₅. For example, the PEDOT coating guarantees a short

transfer/transport distance and electrolyte accessibility for electrons and ions in a core-shell structure, 43 which can also be found in α-Fe₂O₃/PEDOT nanoparticles for supercapacitors. 44 Gradient oxygen vacancies formed in G-V₂O₅/ PEDOT, and some V⁵⁺ species were reduced to V⁴⁺ and further to V^{3+} during the PEDOT formation. The presence of oxygen vacancies and corresponding low-valence vanadium cations (V4+ and V3+) at the surface benefits the charge transfer/transport and redox reactions (proved by theoretical calculations in the next paragraph). With V4+ and V3+ created at the subsurface and V⁵⁺ inside the V₂O₅-NF, gradient oxygen vacancies likely facilitate the charge transfer kinetics and promote the redox reactions at the surface of V2O5-NF with little or no sacrifice of the storage capacitance. The presence of gradient oxygen vacancies at the surface also helps to preserve the morphology integrity by reducing stress and the electrostatic repulsion between adjacent oxygen layers, and to provide vacancies for ion intercalation and a microchannel for charge transfer, 27,38 as reported in α -MoO₃. Nevertheless, it should be mentioned that $V_2O_5/PEDOT$ nanosheets with conformal PEDOT coating ^{4.5} exhibited different properties when prepared by oxidative polymerization, but in solution. Without forming oxygen vacancies, V₂O₅/PEDOT nanosheet-based supercapacitors (tested under the same electrolyte) present a specific capacitance of about 325 F g⁻¹ at 0.5 A g⁻¹ and energy density of 28.9 W h kg⁻¹. These values are higher than that of V_2O_5 -NF in this work (251 F g⁻¹ at 0.5 A g⁻¹, 44 W h kg⁻¹), which suggests the contribution of PEDOT shells to the improved electrochemical performance. However, the performance of V₂O₅/PEDOT nanosheets without oxygen vacancies is still much farther from that of G-V₂O₅/PEDOT nanocables in this work (614 F g^{-1} at 0.5 A g^{-1} , 85 W h kg^{-1}). Therefore, the gradient oxygen vacancies and PEDOT shells synergistically render G-V₂O₅/PEDOT with excellent performance.

Considering the fact that it is difficult to experimentally separate the gradient oxygen vacancies from PEDOT without involving new oxidants, theoretical calculations were performed. The terminal vanadium oxygen vacancies can facilitate electron transfer at the interface, which is proved by detailed density functional theory calculations (the Supporting Information and Figure S5). The density of states (DOS) for V_2O_5 and oxygen vacancy-containing V_2O_5 are shown in Figure 3f. The oxygen vacancy-containing V₂O₅ (001) plane exhibits a semiconducting characteristic with a band gap of 1.23 eV, smaller than that of bulk V_2O_5 , which was also detected by others. 46 The DOS for the V_2O_5 (001) plane with isolated surface defects lowers the bottom of the conduction band to -0.4 eV, resulting in metallic character as observed in Figure 3f. After removal of the vanadyl oxygen, V⁴⁺–O–V⁴⁺ forms between the surface vanadium site (vanadium in vanadyl, position A) and the vanadyl group of the layer beneath (position B). More specifically, a projected density of states (PDOS) calculation for the surface vanadium in vanadyl (position A) in Figure 3g indicates that the excess electrons localize at the V sites and occupy V 3d states at the bottom of the conduction band.

Cycling life is another important parameter for high-performance pseudocapacitors because instability of $\rm V_2O_5$ is another main factor limiting its practical application. To this aim, the cycling performance of $\rm G\text{-}V_2O_5/PEDOT$ was tested under a current density of 10 A g⁻¹ (Figure 3h). $\rm G\text{-}V_2O_5/PEDOT$ nanocables display a long-time cycling durability with 122% of the original specific capacitance retained after 50 000

charge/discharge cycles, and the cycling performance is repeatable and reproducible, while the specific capacitance of $V_2 O_5$ -NF retains only 71% after 2000 charge/discharge cycles (inserted in Figure 3h). The cycling performance of G-V $_2$ O $_5$ /PEDOT is also better than values reported by others, support array (96% retention after 20 000 cycles), 47 MnO $_2$ /PEDOT (93% retention after 5000 cycles), 48 V $_2$ O $_5$ /PANI (92% retention after 5000 cycles), 49 and V $_2$ O $_5$ /PPy (73% retention after 2000 cycles). 50

The morphologies of cycled G-V₂O₅/PEDOT and cycled V₂O₅-NF electrodes were studied. As shown in SEM images in Figure 4a,b, most V₂O₅-NF species dissolve from nanofibers into nanoparticles, and their structure collapses. This reveals their electrochemical reactions with a longer transfer distance for electrons and leads to rapid collapse of effective capacitance of supercapacitors (71% retention after 2000 cycles in Figure 3h). In contrast to V₂O₅-NF, the morphology integrity of G-V₂O₅/PEDOT nanocables is preserved and structural pulverization is restrained after 50 000 cycles (Figure 4b). Further explorations reveal that the core-shell structure of G-V₂O₅/ PEDOT nanocables is still well-retained, as shown in TEM images (Figures 4c,d), EDS line profile, and element mapping profiles (Figure 4e). Although the PEDOT shell appears to change slightly with a partially rough surface (in red circles) and with thickness ranging from 3.5 to 5.0 nm, the PEDOT shell is still tightly attached to the V₂O₅-NF core. This suggests that the PEDOT shell works as a protective layer to prevent V₂O₅-NF from being directly exposed to the electrolyte, shielding V₂O₅-NF from structurally disintegrating during charging and discharging processes.⁵⁴ The increased specific capacitance also suggests a minimal contribution of PEDOT shells to the specific capacitance of G-V₂O₅/PEDOT.

Oxygen vacancies in a cycled G-V₂O₅/PEDOT electrode were analyzed by V 2p2/3 XPS spectra (Figure 4f). There are noticeable changes in vanadium valence states after 50 000 cycles as presented in Table 2. The content of V⁵⁺ increases

Table 2. Contents of Various Vanadium Valence States in G-V₂O₅/PEDOT Electrode after 50 000 Cycles

sample	V^{5+}	V^{4+}	V^{3+}
G-V ₂ O ₅ /PEDOT	52.1%	40.6%	7.3%
cycled G-V ₂ O ₅ /PEDOT	61.0%	30.2%	8.8%

from 52.1% to 61.0% along with a relative decrease of V⁴⁺ from 40.6% to 30.2%, while the amount of V3+ changes slightly from 7.3% to 8.8%. The total vanadium valence calculated from XPS data increases from 4.4 to 4.5. Such a change in redistribution of vanadium cations with different valence states seems to suggest some migration and redistribution of oxygen vacancies during the charge/discharge processes. The gradient oxygen vacancies are induced in a low processing temperature, so the diffusion of oxygen vacancies is limited for G-V₂O₅/PEDOT. As depicted in Figure 4g, when the electrochemical performance was measured with a voltage applied, the electric field would assist and promote the migration of oxygen vacancies and reduce the concentration gradient at the surface. As the XPS is only capable of characterizing a very shallow surface layer, the decreased concentration in V4+ compensated by an increased concentration of VS+ can be explained as an inward migration of oxygen vacancies, with a more homogeneous distribution of oxygen vacancies. Since the amount of oxygen vacancies in G-V₂O₅/PEDOT remains unchanged and the concentration of V^{5+} increases at the surface, there are more V^{5+} species available for redox reactions, resulting in the increased capacitance in the long cycling process. The gradient oxygen vacancies at the surface can also help to preserve the morphology integrity as discussed above. Thus, the excellent cyclic performance of $G\text{-}V_2O_5/\text{PEDOT}$ is attributed to the synergy of gradient oxygen vacancies and the PEODT coating (discussed above). Since the polymerization of PEDOT can be controlled by synthesis conditions, such as polymerization time, 43 the control of gradient oxygen vacancies will be our future work to further explore their effects on energy storage materials.

4. CONCLUSIONS

A gradient distribution of oxygen vacancies was induced into G-V₂O₅/PEDOT nanocables by vapor-phase polymerization. The concentration of oxygen vacancies decreased from the surface of V₂O₅-NF to the core, due to the oxidative polymerization of PEDOT on the V₂O₅-NF surface. The charge transfer kinetics of G-V₂O₅/PEDOT nanocables was significantly enhanced after the formation of gradient oxygen vacancies, which was proven by density functional theory calculations. Thus, G-V₂O₅/PEDOT nanocables exhibited a high specific capacitance of 614 F g⁻¹ and energy density of 85 W h kg⁻¹ when applied in supercapacitors. With the synergistic effects of gradient oxygen vacancies and the PEDOT shell, the structural disintegration of G-V₂O₅/PEDOT nanocables was suppressed effectively, and a steadily increased capacitance was obtained with 122% capacitance retention over 50 000 cycles as oxygen vacancies migrated and redistributed during the charge/discharge processes. This synthesis of ordered oxygen vacancies has potential for preparing electrode materials for high-performance supercapacitors.

ASSOCIATED CONTENT

Supporting Information

The Supporting Information is available free of charge on the ACS Publications website at DOI: 10.1021/acsaem.8b01676.

XANES measurement information, SEM and TEM images for V_2O_5 -NF, TG-DSC curves for $G-V_2O_5$ /PEDOT, and CV and galvanostatic charge/discharge curves for $G-V_2O_5$ /PEDOT, V_2O_5 -NF, and raw V_2O_5 powder (PDF)

AUTHOR INFORMATION

Corresponding Authors

*E-mail: gao@tongji.edu.cn (G.G).

*E-mail: wugm@tongji.edu.cn (G.W).

*E-mail: gzcao@u.washington.edu (G.C).

ORCID ®

Guozhong Cao: 0000-0001-6539-0490

Notes

The authors declare no competing financial interest.

ACKNOWLEDGMENTS

The authors W.B., Y.W., J.W., Y.D., G.G., and G.W. acknowledge the support of the National Natural Science Foundation of China (Grants U1503292, 51472182), the Fundamental Research Funds for the Central Universities, and the National Key Research and Development Program of China (Grant 2017YFA0204600). The authors W.B, C.L., and

G.C. were also supported by the National Science Foundation (DMR 1505902, 1803256). W.B. like to acknowledge the scholarship from the China Scholarship Council (CSC) for the opportunity to study at the University of Washington. W.B. and G.C. gratefully acknowledge the XANES measurement support provided by Gerald T. Seidle and Evan P. Jahrman from University of Washington.

REFERENCES

- (1) Chu, S.; Majumdar, A. Opportunities and Challenges for A Sustainable Energy Future. *Nature* **2012**, *488*, 294–303.
- (2) Cao, F.; Zhao, M.; Yu, Y.; Chen, B.; Huang, Y.; Yang, J.; Cao, X.; Lu, Q.; Zhang, X.; Zhang, Z.; Tan, C.; Zhang, H. Synthesis of Two-Dimensional CoS1.097/Nitrogen-Doped Carbon Nanocomposites Using Metal-Organic Framework Nanosheets as Precursors for Supercapacitor Application. J. Am. Chem. Soc. 2016, 138, 6924—7.
- (3) Mai, L. Q.; Minhas-Khan, A.; Tian, X.; Hercule, K. M.; Zhao, Y. L.; Lin, X.; Xu, X. Synergistic interaction between redox-active electrolyte and binder-free functionalized carbon for ultrahigh supercapacitor performance. *Nat. Commun.* **2013**, *4*, 2923.
- (4) Cao, X.; Zheng, B.; Shi, W.; Yang, J.; Fan, Z.; Luo, Z.; Rui, X.; Chen, B.; Yan, Q.; Zhang, H. Reduced graphene oxide-wrapped MoO3 composites prepared by using metal-organic frameworks as precursor for all-solid-state flexible supercapacitors. *Adv. Mater.* **2015**, 27, 4695–701.
- (5) Owusu, K. A.; Qu, L.; Li, J.; Wang, Z.; Zhao, K.; Yang, C.; Hercule, K. M.; Lin, C.; Shi, C.; Wei, Q.; Zhou, L.; Mai, L. Low-crystalline iron oxide hydroxide nanoparticle anode for high-performance supercapacitors. *Nat. Commun.* **2017**, *8*, 14264.
- (6) Sun, G.; Zhang, X.; Lin, R.; Chen, B.; Zheng, L.; Huang, X.; Huang, L.; Huang, W.; Zhang, H.; Chen, P. Weavable, High-Performance, Solid-State Supercapacitors Based on Hybrid Fibers Made of Sandwiched Structure of MWCNT/rGO/MWCNT. Adv. Electron. Mater. 2016, 2, 1600102.
- (7) Simon, P.; Gogotsi, Y. Materials for Electrochemical Capacitors. *Nat. Mater.* **2008**, *7*, 845–54.
- (8) He, G.; Ling, M.; Han, X.; Abou El Amaiem, D. I.; Shao, Y.; Li, Y.; Li, W.; Ji, S.; Li, B.; Lu, Y.; Zou, R.; Ryan Wang, F.; Brett, D. J. L.; Xiao Guo, Z.; Blackman, C.; Parkin, I. P. Self-Standing Electrodes with Core-Shell Structures for High-Performance Supercapacitors. *Energy Storage Mater.* **2017**, *9*, 119–125.
- (9) Sun, G.; Zhang, X.; Lin, R.; Yang, J.; Zhang, H.; Chen, P. Hybrid fibers made of molybdenum disulfide, reduced graphene oxide, and multi-walled carbon nanotubes for solid-state, flexible, asymmetric supercapacitors. *Angew. Chem., Int. Ed.* **2015**, *54*, 4651–6.
- (10) Jiang, H.; Lee, P. S.; Li, C. Z. 3D Carbon Based Nanostructures for Advanced Supercapacitors. *Energy Environ. Sci.* **2013**, *6*, 41–53.
- (11) Snook, G. A.; Kao, P.; Best, A. S. Conducting-Polymer-Based Supercapacitor Devices and Electrodes. *J. Power Sources* **2011**, *196*, 1–12
- (12) Ratajczak, P.; Suss, M. E.; Kaasik, F.; Béguin, F. Carbon Electrodes for Capacitive Technologies. *Energy Storage Mater.* **2019**, 16, 126–145.
- (13) Jiang, J.; Li, Y.; Liu, J.; Huang, X.; Yuan, C.; Lou, X. W. Recent Advances in Metal Oxide-Based Electrode Architecture Design for Electrochemical Energy Storage. *Adv. Mater.* **2012**, *24*, 5166–80.
- (14) Yao, J.; Li, Y.; Massé, R. C.; Uchaker, E.; Cao, G. Revitalized interest in vanadium pentoxide as cathode material for lithium-ion batteries and beyond. *Energy Storage Mater.* **2018**, *11*, 205–259.
- (15) Zhi, M. J.; Xiang, C. C.; Li, J. T.; Li, M.; Wu, N. Q. Nanostructured Carbon-Metal Oxide Composite Electrodes for Supercapacitors: A Review. *Nanoscale* **2013**, *5*, 72–88.
- (16) Qu, Q. T.; Shi, Y.; Li, L. L.; Guo, W. L.; Wu, Y. P.; Zhang, H. P.; Guan, S. Y.; Holze, R. V₂O₅·0.6H₂O Nanoribbons as Cathode Material for Asymmetric Supercapacitor in K₂SO₄ Solution. *Electrochem. Commun.* **2009**, 11, 1325–1328.
- (17) Chen, Z.; Augustyn, V.; Wen, J.; Zhang, Y.; Shen, M.; Dunn, B.; Lu, Y. High-Performance Supercapacitors Based on Intertwined

Н

- (18) Wang, Y.; Cao, G. Z. Developments in Nanostructured Cathode Materials for High-Performance Lithium-Ion Batteries. *Adv. Mater.* **2008**, 20, 2251–2269.
- (19) Perera, S. D.; Patel, B.; Nijem, N.; Roodenko, K.; Seitz, O.; Ferraris, J. P.; Chabal, Y. J.; Balkus, K. J. Vanadium Oxide Nanowire-Carbon Nanotube Binder-Free Flexible Electrodes for Supercapacitors. *Adv. Energy Mater.* **2011**, *1*, 936–945.
- (20) Yan, Y.; Li, B.; Guo, W.; Pang, H.; Xue, H. Vanadium Based Materials as Electrode Materials for High Performance Supercapacitors. *J. Power Sources* **2016**, 329, 148–169.
- (21) Song, Y.; Liu, T. Y.; Yao, B.; Kou, T. Y.; Feng, D. Y.; Liu, X. X.; Li, Y. Amorphous Mixed-Valence Vanadium Oxide/Exfoliated Carbon Cloth Structure Shows a Record High Cycling Stability. *Small* **2017**, *13*, 1700067.
- (22) Engstrom, A. M.; Doyle, F. M. Exploring the Cycle Behavior of Electrodeposited Vanadium Oxide Electrochemical Capacitor Electrodes in Various Aqueous Environments. *J. Power Sources* **2013**, 228, 120–131.
- (23) Wang, G. M.; Lu, X. H.; Ling, Y. C.; Zhai, T.; Wang, H. Y.; Tong, Y. X.; Li, Y. LiCl/PVA Gel Electrolyte Stabilizes Vanadium Oxide Nanowire Electrodes for Pseudocapacitors. *ACS Nano* **2012**, *6*, 10296–10302.
- (24) Liu, P. C.; Zhu, K. J.; Gao, Y. F.; Luo, H. J.; Lu, L. Recent Progress in the Applications of Vanadium-Based Oxides on Energy Storage: from Low-Dimensional Nanomaterials Synthesis to 3D Micro/Nano-Structures and Free-Standing Electrodes Fabrication. *Adv. Energy Mater.* **2017**, *7*, 1700547.
- (25) Kim, H. S.; Cook, J. B.; Lin, H.; Ko, J. S.; Tolbert, S. H.; Ozolins, V.; Dunn, B. Oxygen Vacancies Enhance Pseudocapacitive Charge Storage Properties of MoO_{3-x}. *Nat. Mater.* **2017**, *16*, 454–460.
- (26) Fu, Y.; Gao, X.; Zha, D.; Zhu, J.; Ouyang, X.; Wang, X. Yolk—Shell-Structured MnO₂ Microspheres with Oxygen Vacancies for High-Performance Supercapacitors. *J. Mater. Chem. A* **2018**, *6*, 1601—1611
- (27) Liu, D.; Liu, Y.; Garcia, B. B.; Zhang, Q.; Pan, A.; Jeong, Y.-H.; Cao, G. V_2O_5 Xerogel Electrodes with Much Enhanced Lithium-Ion Intercalation Properties with N_2 Annealing. *J. Mater. Chem.* **2009**, *19*, 8789.
- (28) Liu, D.; Liu, Y.; Pan, A.; Nagle, K. P.; Seidler, G. T.; Jeong, Y.-H.; Cao, G. Enhanced Lithium-Ion Intercalation Properties of V_2O_5 Xerogel Electrodes with Surface Defects. *J. Phys. Chem. C* **2011**, *115*, 4959–4965.
- (29) Yu, M.; Zeng, Y.; Han, Y.; Cheng, X.; Zhao, W.; Liang, C.; Tong, Y.; Tang, H.; Lu, X. Valence-Optimized Vanadium Oxide Supercapacitor Electrodes Exhibit Ultrahigh Capacitance and Super-Long Cyclic Durability of 100 000 Cycles. *Adv. Funct. Mater.* **2015**, 25, 3534–3540.
- (30) Song, H.; Liu, C.; Zhang, C.; Cao, G. Self-doped V^{4+} - V_2O_5 Nanoflake for 2 Li-ion Intercalation with Enhanced Rate and Cycling Performance. *Nano Energy* **2016**, 22, 1–10.
- (31) Qu, Q. T.; Zhu, Y. S.; Gao, X. W.; Wu, Y. Core-Shell Structure of Polypyrrole Grown on V₂O₅ Nanoribbon as High Performance Anode Material for Supercapacitors. *Adv. Energy Mater.* **2012**, *2*, 950–955.
- (32) Wu, Y. J.; Gao, G. H.; Wu, G. M. Self-assembled Three-Dimensional Hierarchical Porous V₂O₅/graphene Hybrid Aerogels for Supercapacitors with High Energy Density and Long Cycle Life. *J. Mater. Chem. A* **2015**, *3*, 1828–1832.
- (33) Stoller, M. D.; Ruoff, R. S. Best Practice Methods for Determining an Electrode Material's Performance for Ultracapacitors. *Energy Environ. Sci.* **2010**, *3*, 1294–1301.
- (34) Wu, Y. J.; Gao, G. H.; Yang, H. Y.; Bi, W.; Liang, X.; Zhang, Y.; Zhang, G.; Wu, G. Controlled Synthesis of V₂O₅/MWCNT Core/Shell Hybrid Aerogels through a Mixed Growth and Self-Assembly Methodology for Supercapacitors with High Capacitance and Ultralong Cycle Life. *J. Mater. Chem. A* **2015**, *3*, 15692–15699.

- (35) Bi, W.; Gao, G.; Wu, Y.; Yang, H.; Wang, J.; Zhang, Y.; Liang, X.; Liu, Y.; Wu, G. Novel Three-Dimensional Island-Chain Structured V_2O_5 /Graphene/MWCNT Hybrid Aerogels for Supercapacitors with Ultralong Cycle Life. *RSC Adv.* **2017**, *7*, 7179–7187.
- (36) Zhou, X. W.; Wu, G. M.; Wu, J. D.; Yang, H.; Wang, J.; Gao, G.; Cai, R.; Yan, Q. Multiwalled Carbon Nanotubes–V₂O₅ Integrated Composite with Nanosized Architecture as A Cathode Material for High Performance Lithium Ion Batteries. *J. Mater. Chem. A* **2013**, 1, 15459–15468.
- (37) Jiang, C.; Chen, G.; Wang, X. High-Conversion Synthesis of Poly(3,4-Ethylenedioxythiophene) by Chemical Oxidative Polymerization. *Synth. Met.* **2012**, *162*, 1968–1971.
- (38) Wu, Q. H.; Thissen, A.; Jaegermann, W.; Liu, M. L. Photoelectron Spectroscopy Study of Oxygen Vacancy on Vanadium Oxides Surface. *Appl. Surf. Sci.* **2004**, 236, 473–478.
- (39) Lock, J. P.; Im, S. G.; Gleason, K. K. Oxidative Chemical Vapor Deposition of Electrically Conducting Poly(3,4-ethylenedioxythiophene) Films. *Macromolecules* **2006**, 39, 5326–5329.
- (40) Scanlon, D. O.; Walsh, A.; Morgan, B. J.; Watson, G. W. An ab initio Study of Reduction of V_2O_5 through the Formation of Oxygen Vacancies and Li Intercalation. *J. Phys. Chem. C* **2008**, *112*, 9903–9911.
- (41) Seidler, G. T.; Mortensen, D. R.; Remesnik, A. J.; Pacold, J. I.; Ball, N. A.; Barry, N.; Styczinski, M.; Hoidn, O. R. A laboratory-based hard x-ray monochromator for high-resolution x-ray emission spectroscopy and x-ray absorption near edge structure measurements. *Rev. Sci. Instrum.* **2014**, *85*, 113906.
- (42) Xu, Y.; Zhou, M.; Zhang, C.; Wang, C.; Liang, L.; Fang, Y.; Wu, M.; Cheng, L.; Lei, Y. Oxygen Vacancies: Effective Strategy to Boost Sodium Storage of Amorphous Electrode Materials. *Nano Energy* **2017**, 38, 304–312.
- (43) Mai, L. Q.; Dong, F.; Xu, X.; Luo, Y.; An, Q.; Zhao, Y.; Pan, J.; Yang, J. Cucumber-like V₂O₅/poly(3,4-ethylenedioxythiophene) &MnO₂ Nanowires with Enhanced Electrochemical Cyclability. *Nano Lett.* **2013**, *13*, 740–745.
- (44) Park, J. W.; Na, W.; Jang, J. Hierarchical Core/Shell Janus-type α-Fe₂O₃/PEDOT Nanoparticles for High Performance Flexible Energy Storage Devices. *J. Mater. Chem. A* **2016**, *4*, 8263–8271.
- (45) Guo, C. X.; Yilmaz, G.; Chen, S.; Chen, S.; Lu, X. Hierarchical Nanocomposite Composed of Layered V₂O₅/PEDOT/MnO₂ Nanosheets for High-performance Asymmetric Supercapacitors. *Nano Energy* **2015**, *12*, 76–87.
- (46) Blum, R. P.; Niehus, H.; Hucho, C.; Fortrie, R.; Ganduglia-Pirovano, M. V.; Sauer, J.; Shaikhutdinov, S.; Freund, H. J. Surface Metal-Insulator Transition on A Vanadium Pentoxide (001) Single Crystal. *Phys. Rev. Lett.* **2007**, *99*, 226103.
- (47) Xie, Q.; Xu, Y.; Wang, Z.; Xu, C.; Zou, P.; Lin, Z.; Xu, C.; Yang, C.; Kang, F.; Wong, C. P. Vapor-Phase Polymerized Poly(3,4-Ethylenedioxythiophene) on a Nickel Nanowire Array Film: Aqueous Symmetrical Pseudocapacitors with Superior Performance. PLoS One 2016, 11, No. e0166529.
- (48) Tang, P.; Han, L.; Zhang, L.; Wang, S.; Feng, W.; Xu, G.; Zhang, L. Controlled Construction of Hierarchical Nanocomposites Consisting of MnO₂ and PEDOT for High-Performance Supercapacitor Applications. *ChemElectroChem* **2015**, *2*, 949–957.
- (49) Bai, M. H.; Liu, T. Y.; Luan, F.; Li, Y.; Liu, X.-X. Electrodeposition of Vanadium Oxide—Polyaniline Composite Nanowire Electrodes for High Energy Density Supercapacitors. J. Mater. Chem. A 2014, 2, 10882—10888.
- (50) Bai, M. H.; Bian, L. J.; Song, Y.; Liu, X. X. Electrochemical Codeposition of Vanadium Oxide and Polypyrrole for High-Performance Supercapacitor with High Working Voltage. *ACS Appl. Mater. Interfaces* **2014**, *6*, 12656–64.
- (51) Cao, L.; Zhu, J.; Li, Y.; Xiao, P.; Zhang, Y.; Zhang, S.; Yang, S. Ultrathin Single-Crystalline Vanadium Pentoxide Nanoribbon Constructed 3D Networks for Superior Energy Storage. *J. Mater. Chem. A* **2014**, *2*, 13136–13142.
- (S2) Qian, T.; Xu, N.; Zhou, J. Q.; Yang, T. Z.; Liu, X. J.; Shen, X. W.; Liang, J. Q.; Yan, C. L. Interconnected Three-Dimensional $V_2O_5/$

ı

ACS Applied Energy Materials

Polypyrrole Network Nanostructures for High Performance Solid-State Supercapacitors. *J. Mater. Chem. A* **2015**, *3*, 488–493.

(53) Chen, Z.; Qin, Y.; Weng, D.; Xiao, Q.; Peng, Y.; Wang, X.; Li, H.; Wei, F.; Lu, Y. Design and Synthesis of Hierarchical Nanowire Composites for Electrochemical Energy Storage. *Adv. Funct. Mater.* **2009**, *19*, 3420–3426.

(54) Chao, D.; Xia, X.; Liu, J.; Fan, Z.; Ng, C. F.; Lin, J.; Zhang, H.; Shen, Z. X.; Fan, H. J. A $\rm V_2O_5/Conductive$ -Polymer Core/Shell Nanobelt Array on Three-Dimensional Graphite Foam: A High-Rate, Ultrastable, and Freestanding Cathode for Lithium-Ion Batteries. *Adv. Mater.* **2014**, *26*, 5794–800.



This document was created with the Win2PDF "print to PDF" printer available at http://www.win2pdf.com

This version of Win2PDF 10 is for evaluation and non-commercial use only.

This page will not be added after purchasing Win2PDF.

http://www.win2pdf.com/purchase/